Exploring metamagnetism in triangular Ising networks: Insights from further-neighbor interactions with a case study on ErGa₂

Po-Hao Chang [*] and Igor I. Mazin [†]

Department of Physics and Astronomy, George Mason University, Fairfax, Virginia 22030, USA
and Quantum Science and Engineering Center, George Mason University, Fairfax, Virginia 22030, USA

Recent attention to frustrated magnetism has revived interest in most fundamental models of the latter, such as the classical triangular Ising lattice (I-3). Despite the long history, our understanding of the physics of I-3 is still patchy, and even the mean-field magnetic phase diagram has been addressed only in specific cases. Here we present a study considerably more exhaustive than those available in the literature, including arbitrary Heisenberg interaction up to 4th nearest neighbors (NN) identifying all inequivalent magnetic patterns up to the 8th NN (1901 of those), and calculating the phase diagrams in the external magnetic field. We then connect these findings with a real-life material, ErGa₂, which our calculations show to be a very good approximation to the I-3, despite its crystallographically 3D character. We calculate, from first principles, the exchange parameters, and show that they reproduce well the observed magnetization steps. We also find a possibility of additional narrow steps, which may be observed in future experiments.

I. INTRODUCTION

There has been recent interest in 2-dimensional magnetic systems as they are often candidates for nontrivial magnetic states, such as spin liquids [1–4]. Considerable progress has been achieved regarding insulating 2D kagome lattices dominated by short-range interactions [5]. Magnetic anisotropy in such systems is small, and the continuous degeneracy of magnetic order plays an important role.

A relatively recent addition to this landscape is rare-earth-based systems [6] with a strong uniaxial anisotropy, dominating over a relatively weak exchange. Interesting physics there comes from the fact that, on one hand, the Ising model on a kagome lattice does not show a phase transition (as opposed to the famous square lattice [7]), and, on the other hand, when embedded in a good metal background the rare-earth ions show a relatively weak but long-range and potentially sign-changing exchange interaction (related to the Rudermann-Kittel-Kasuya-Yosida, RKKY, interaction [8–10]). This leads to these materials exhibiting a number of metamagnetic transitions, that is, discrete steps in magnetization as a function of magnetic field, ranging from two to as many as nine steps.

In this case, the strong geometric frustration associated with the kagome lattice is not necessary (albeit may be helpful). The simple triangular, not really frustrated in Heisenberg or XY models, where the ground state is uniquely defined as a 120° spin star, is frustrated in the sense of an infinitely degenerate discontinuous ground state, in the classical Ising model [11].

The classical Ising model on the triangular lattice (I-3), while simple in the nearest-neighbors (NN) only approximation, becomes increasingly richer and more complex when further interactions are added [12–15]. For instance, in Refs. [12–15] some possible ground state orders were identified, upon including up to the fifth nearest neighbors. However, the studies so far have not been sufficiently exhaustive, even within a limited interaction range, nor has any attempt been made to estimate how realistic the parameter ranges that generate strong metamagnetism with a large number of magnetization steps are.

In this paper, we identify one such candidate, ErGa₂ [the structure shown in Fig. 1(a)], a material known since the 1970s [16,17] and having one strong magnetization step [16–20], albeit some narrow steps below and above cannot be confidently excluded. It is known, and we can confirm the same computationally, to have an easy axis perpendicular to the triangular Er plane, with a strong anisotropy [22,23], with the large magnetic moment of 9.5 μ_B [16–20]. Our calculations also show a strong NN ferromagnetic interaction perpendicular to *ab* plane, making it a perfect implementation of the classical I-3 model.

The paper is organized as follows. First, since we believe that, despite a number of papers on long-range triangular Ising the full phase diagram has not been established and its complexity is not appreciated, in the first part, we study the I-3 model with up to the 3rd nearest neighbors in a range of parameters J_2 and J_3 (J_1 in this part is set to 1), and in some cases adding a rather small J_4 in order to reveal new phases otherwise degenerate with some others. The richest phase diagram is observed when all interactions are antiferromagnetic (AF); this case is discussed in Sec. III. Subsequently, a more realistic case, inspired by RKKY and by our calculations for ErGa₂, where $J_1, J_2 > 0$ (antiferromagnetic) and
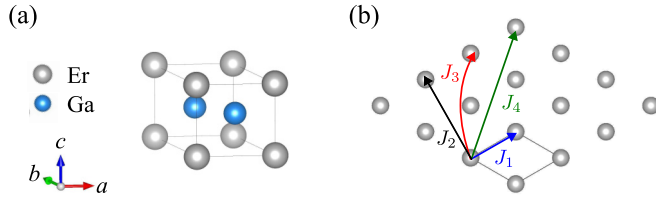
FIG. 1. (a) Crystal structure of ErGa$_2$. (b) Effective 2D triangular lattice.

$J_1, J_2 < 0$ (ferromagnetic), is presented. Next, we present our first-principles calculations of J_{1-4} in ErGa$_2$ and compared the phase diagram in the regime corresponding to the calculated values (as well as "around" them, to account for possible inaccuracy in DFT calculations).

II. GENERAL MODEL

The model magnetic Hamiltonian of up to fourth nearest neighbor (4NN) in the presence of an external magnetic field is as follows:

$$H = \sum_{\langle ij \rangle_1} J_1 m_i^z m_j^z + \sum_{\langle ij \rangle_2} J_2 m_i^z m_j^z$$
$$+ \sum_{\langle ij \rangle_3} J_3 m_i^z m_j^z + \sum_{\langle ij \rangle_4} J_4 m_i^z m_j^z - h \sum_i m_i, \qquad (1)$$

where m are the normalized moments ($\mathbf{m} = \mathbf{S}/|S|$, $|\mathbf{m}| = 1$), J_i are the exchange parameters of the ith NN ($i = 1$–4) defined in Fig. 1(b), and $h = H_{\text{ext}}M$ is the Zeeman energy in the external field $H_{\text{ext}} \| z$. In particular, in the later discussed case of ErGa$_2$, this approach is justified by the fact that the calculated Er magnetic moments depend very little on the assumed magnetic pattern.

Since finding a new ground state is generally not a trivial task, particularly when more further neighbors are included, in our study, we adopted a similar approach to Ref. [24] for energy comparison across a predetermined set of possible magnetic patterns. To construct this set, however, instead of a semi-intuitive approach as in the previous studies, we have developed a protocol for a systematic search to identify all inequivalent orderings for any supercell up to a given size. In what we report below, the maximum length of the lattice vectors used to construct the cell is limited to the 8th-NN distance (16.744 Å in ErGa$_2$). The algorithm yielded 1910 inequivalent spin Hamiltonians [i.e., excluding patterns having the same Hamiltonian Eq. (1) with nonzero J_{1-4}]. In addition, we also included one particular pattern outside of our cutoff that has been suggested in the earlier study by Tanaka [12]. Then, the phase diagrams were obtained by identifying the configuration with the lowest energy for every parameter set (i.e., h and J_i).

Figure 2 selectively displays states explicitly discussed in this paper. For a comprehensive compilation of magnetic patterns identified as ground states or closely approaching ground state energies, please refer to the Supplemental Material [21]. Each state is labeled with a number preceded by the "#" sign as defined in both Fig. 2 and the Supplemental Material.

In our first-principles-based analysis, we calculated the total energies for seven different magnetic orderings, #1, #2,

#3, #4, #5, #9, and #12, as shown in Fig. 2. The data were then fitted to Eq. (1) to extract exchange parameters J_{1-4}^{DFT}. The total energy for each configuration was calculated using the Vienna *ab initio* Simulation Package (VASP) [25] within the projector augmented wave (PAW) method [26,27]. The Perdew-Burke-Ernzerhof (PBE) [28] generalized gradient approximation was employed to describe exchange-correlation effects. The on-site Coulomb interactions are taken into account using LDA+U [29] to improve the description of the interactions between the localized f electrons of Er. A large $U - J = 8$ was used. The experimental lattice parameters $a = 4.1861$ and $c = 4.0187$ Å taken from Ref. [17] were used in all the calculations.

Due to the small energy scale associated with the exchange interactions, additional care was taken to ensure proper energy convergence concerning the k-point mesh. For the out-of-plane components, since we assume all the layers to be equivalent, a sufficiently large $k_z = 13$ is used for all calculations. On the other hand, numerical errors can arise from the comparison between different in-plane cell shapes. To mitigate the inconsistencies in the corresponding k-space integration, the ferromagnetic state was evaluated for all cell shapes involved (i.e., #1, #2, #5, #9, and #12), and the k-point mesh was increased progressively until the energy difference between any given state and the FM state converged to 10^{-4} eV.

III. GENERAL DISCUSSION

Case 1: J_1, J_2, J_3, and $J_4 > 0$

In the first part, we consider the most frustrated case where all the magnetic moments are antiferromagnetically coupled to each other (i.e., all $J_i > 0$) with the 4NN only added to lift the observed degeneracies. Figure 3(a) shows the phase diagram for $J_3 = 0$ which corresponds to the 2NN case. There are four major stable phases in the given parameter space. For $J_2 > 0$, only #1 exists without an external field, h, and the rest are induced by h. The ground state at the low field is stripe AF and borders with #2 or #3 depending on the strength of J_2. Along the boundaries separating #1 and #2, #1 and #3, as well as #3 and #4, there are also subtle traces of multiple degenerate states, where a few very tiny points corresponding to phases such as #10 or #17 can be discerned.

To investigate the behavior of the possible degeneracies, we added a small finite $J_3 = 0.02$ as shown in Fig. 3(b). As a result, several very thin straight lines emerge. One in the low-field region ($H \lesssim 3$) corresponds to phase #7, which lies between phases #1 and #2, indicating a triple degeneracy. This degeneracy can be verified analytically by equating the energy of the degenerate states. In this case, the magnetic energies for the degenerate states in the 2NN approximation are

$$E_1 = -1 - J_2, \qquad (2)$$

$$E_2 = -1 + 3J_2 - \tfrac{1}{3}h, \qquad (3)$$

and

$$E_7 = -1 - 1.4J_2 - \tfrac{1}{5}h. \qquad (4)$$

By imposing the condition, $E_1 = E_2 = E_7$, one finds the common solution $H = 12J_2$. It is worth noting that at zero field,
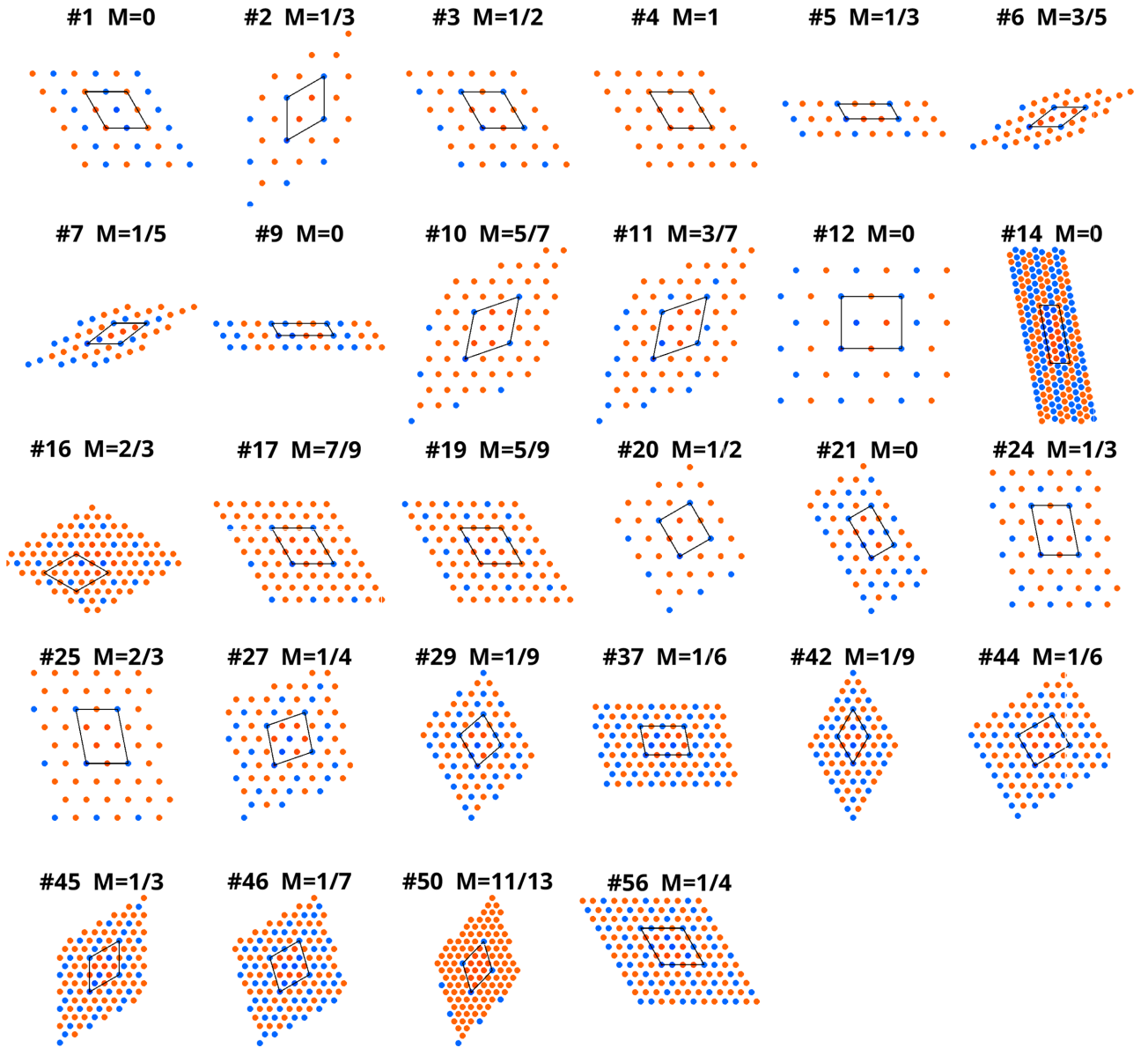
FIG. 2. Possible magnetic ground states and their corresponding magnetization per site under study. Blue and red colors indicate opposite spins. This graph shows only the states explicitly discussed in the text. For a more comprehensive list, please refer to the Supplemental Material [21].

there is a different type of antiferromagnetic (AF) ground state, phase #12. There are also two long parallel lines corresponding to phases #27 and #24 that develop between phases #1 and #3, with phase #37 still degenerate at the #1–#27 boundary. A point of triple degeneracy (#1, #2, and #3) now develops into a new phase (#56) and is surrounded by six different phases, as shown in the inset.

In the high-field region ($H \gtrsim 6$), although the presence of J_3 partially removes the degeneracies between #3 and #4, which, in turn, leads to the emergence of #10, the colored dots that correspond to #17 and #50 (#25) remain degenerate at the #4 and #10 (#3 and #10) border. This shows a *sextuple* degeneracy in the 2NN approximation. By following the same procedure mentioned earlier, one finds the condition for the *sextuple* degeneracy to be $h = 6 + 6J_2$, where #3, #4, #10, #17, #25, and #50 are degenerate.

The state #17 corresponds to the total magnetization $M = 7/9$ and has been observed and discussed in Ref. [14] as its formation requires introducing J_4. Additionally, around $H \sim 6$, a very tiny region (#19) bordering with #2, #3, and #10 starts to emerge.

Adding an even longer range, and an even smaller interaction $J_4 = 0.015$, forces nearly all the J_3-induced phases to disappear except that the tiny region of #19 remains unaffected [see Fig. 3(c)]. In the low-field regime, the disappearance of #7 and #56 is mainly due to the slight expansion of the #2 phase, while #12 at small J_2 around zero field is directly replaced with #42. The rest are replaced with new phases #44 and #45 (#16 and #17) between #1 and #3 (#3 and #4). It is interesting to note that at precisely $H = 0$ the states #21 and #42, despite having different magnetizations— $M = 0$ and $1/9$, respectively—exhibit identical exchange
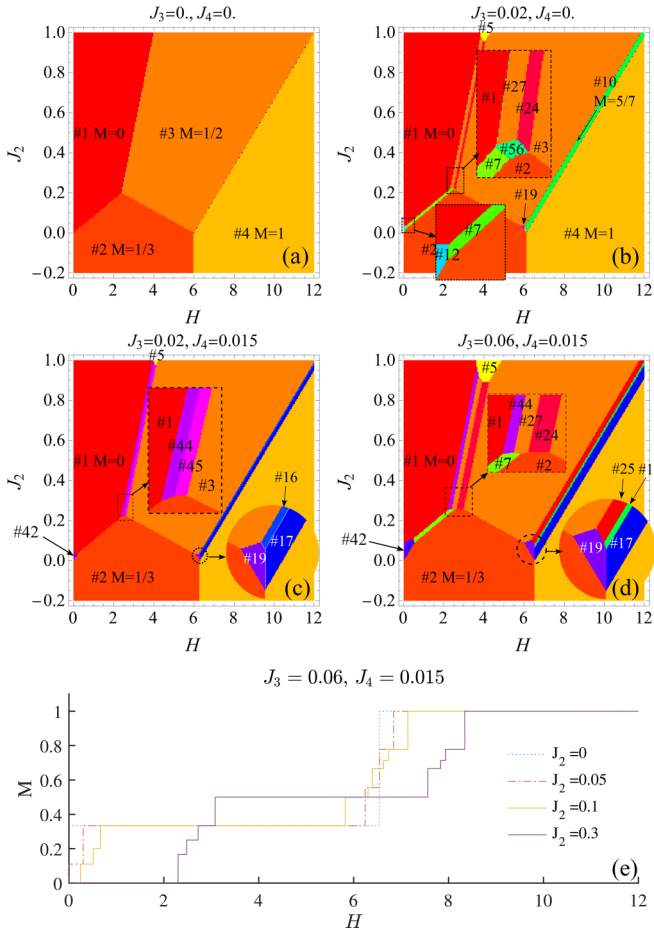
FIG. 3. [(a)–(d)] show the phase diagrams for different weak J_3 and J_4 and (e) M-H curve for $(J_3, J_4) = (0.05, 0.015)$ at several different J_2 as specified in the legend.

FIG. 4. (a), (c), and (d) show the phase diagrams for different weak J_3 and J_4 and (b) M-H curve for $(J_3, J_4) = (0.05, 0.015)$ at several different values of J_2.

Hamiltonians up to the 4th NN. As a result, these states are always degenerate at zero field.

When J_3 increases further to 0.06, as shown in Fig. 3(d), a small region of state #5 at a very large J_2 begins to emerge. The states #7, #24, #27, and #10 reappear along with a new phase #25 and the states #45 and #16, promoted by the small J_4 interaction, are replaced. Two small regions, #19 that is insensitive to the small J_4 as well as #42 that is induced by J_4, begin to expand significantly as the J_3 increases. Interestingly, the long narrow belt-shaped area between #3 and #4 consists of three parallel thin lines running across nearly the entire range of J_2. These thin lines, resulting from the lifting of degeneracy by weak interactions with farther neighbors, appear in the the M-H plots as three successive short steps illustrated in Fig. 3(e), which depicts the field-dependent magnetization for $J_2 = 0$ and three nonzero J_2 values. The shape of these short steps in the high-field region, resulting from the further-neighbor interactions, does not vary with J_2 when $J_2 \gtrsim 0.1$ and persists throughout nearly the entire range.

Similar patterns can also be observed in the smaller field regions ($H \sim 3$) as indicated by the orange and purple lines ($J_2 = 0.1$ and 0.3) as a consequence of J_3 lifting the degeneracy between #1 and #2, or #1 and #3. These trends suggest some delicate competition between J_3 and J_4 as each might

favor particular orderings and many of the states are very close in energy. These short steps are likely to exist in a system with weak further neighbors, but could easily get washed out in an experiment due to defects in the sample. In the later discussion, we will only consider a small fixed $J_4 = 0.015$ simply to lift the obvious degeneracies.

As J_3 increases to 0.1, as shown in Fig. 4(a), the phases induced by further NN interactions, namely #5, #7, #10, #19, and #42, continue to expand. Moreover, phase #12 resurfaces, and many new states emerge, particularly within three smaller regions (marked as a-1, a-2, and a-3) as illustrated in magnified views. Three long parallel stripes between #1 and #3 are shortened from both ends. This shrinkage can be attributed to the expansion of #5 (#7) in the large (small) J_2 region. Concurrently, the emergence of new phases #35 and #56 in the a-2 region further contributes to this phenomenon.

The region between phases #1 and #2 mainly consists of phases #12, #42, and #7. In the more focused region, labeled as a-1, which is characterized by a low field and small J_2, there also exist two other intermediate states, #29 and #46.

On the other hand, along the #3–#4 boundary, three parallel stripes remain. The middle stripe, corresponding to phase #10, is strongly favored by J_3 and expands with increasing J_3, while the other two states, #25 and #17, as well as the trace of

#50, which is still degenerate at the #4 boundary, appear to be unaffected by a moderate increase of J_3.

Interestingly, in the a-3 region, near the point where all three major stable phases #2, #3, and #4 are previously degenerate in the absence of farther NN interaction, more phases are formed. Within this small parameter space and these small field windows, there are 10 developed phases with possibly more phases degenerate at the boundaries.

Figure 4(b) shows the *M-H* curves for three different values of J_2 and $J_3/J_4 = 0.1/0.015$. The field dependency is rather sensitive to J_2. While all three curves have rather complicated transition steps, the richest transition behavior happens when the magnitude of J_2 is roughly comparable to $J_3 = 0.1$, as those complicated phases reside within a-1 and a-3 and are likely to be involved in the competition. As discussed earlier, this is a result of the frustration between different neighbors, which in turn leads to a rich phase diagram in the *M-H* space, which can contain as many as 10 transition steps.

The phase diagrams for $J_3 = 0.3$ and 0.5 are shown in Figs. 4(c) and 4(d), respectively. A few trends emerging at larger J_3 can be summarized as follows. Between $J_3 = 0.1$ and 0.3, the changes are rather dramatic. As J_3 continues to increase, phases #2, #5, #6, #10, #12, #19, #42, and #56 are promoted, primarily in the small J_2 region (except for the phase #10). Meanwhile, the states in the region where $J_2 > 0.3$, particularly #1, #3, and the phases in between, are replaced by a new set of states.

The AF phase #1 in the low-field region is now completely replaced by #12 for small J_2 and replaced by a less common AF phase #14 for large J_2. The latter phase (#14) has been discussed analytically in the early study by Tanaka [12] (the only state outside of our cell structure search, because it is unusually elongated in one direction).

The shrinking of #3 and the replacement of stripe phases can be attributed to the expansion of #5 and #10 as well as the emergence of new phases such as #11, #26, and #33. While there are still small regions of new phases like #40 and #28 that emerge, most of the small intermediate states are suppressed [i.e., in the regions such as a-1, a-2, and a-3 defined in Fig. 4(a)]. This trend becomes more obvious as J_3 increases further.

Between $J_3 = 0.3$ and 0.5 [Figs. 4(c) and 4(d)], the states for $J_2 \lesssim 0.4$ stay roughly the same, despite some mild boundary shifts. For larger J_2, the emergence of #8 in the lower field region ($1 < H < 3$) replaces both #26 and #56 and causes both #5 and #40 to shrink. In the higher field region, state #28 expands rapidly and absorbs all the small states that lie within the small region between #2, #6, and #11.

One can see that in Fig. 4(d), the small fragmented regions between the boundaries have nearly all been suppressed, and larger domains are starting to form. This suggests that the system is considerably less frustrated within this range of parameters.

Case 2: $J_1, J_2 > 0$ and $J_3, J_4 < 0$

Inspired by our DFT calculations for the $ErGa_2$ systems, reported in the next section, this second scenario is expected to mimic the longer-range RKKY-type exchange couplings, where the sign oscillates with distance. We then consider up

to the fourth NN where both J_3 and $J_4 < 0$ (FM). This setup is also more consistent with our DFT data, where the model provides an excellent fitting quality.

In this case, we attempt to explore the behavior in the parameter space around the exchange coupling parameters that are extracted from our first-principles calculations. The phase diagrams are summarized in Fig. 5, where the top row (a)–(c) and bottom row (e)–(h) correspond to $J_3 = -0.1$ and -0.3, respectively, and for each J_3 several selected J_4 values are considered.

We first isolate the effect of J_3 by comparing Figs. 5(a) and 5(e) and Fig. 3(a). We find that J_3 alone does not introduce any new phases but shifts the phase boundaries in favor, strongly, of phases #1, #3, and #4. Due to the ferromagnetic nature of J_3, which reduces the frustration in the system, the multiple degeneracies along the #3 and #4 boundary no longer persist. In Fig. 5, both top and bottom rows (i.e., $J_3 = -0.1$ and -0.3) exhibit similar trends, in the sense that with increasing J_4 new phases are developing in the region of small J_2 and low magnetic field, as well as along the #3 and #4 boundary. This again shows some competition between J_3 and J_4 and one expects rich phase diagrams when J_4 and J_3 are comparable.

The configurations in the top row [i.e., Figs. 5(a)–5(c)] are particularly of interest since a small J_3 is more likely in a real system. When $J_4 = -0.075$ (that is, comparable to J_3), see Fig. 5(b), new phases (#7, #12, and #56) begin to emerge between #1 and #2, similar to those shown in Fig. 3(b), but with the boundaries slightly pushed down due to the effect of a positive J_3. This thin stripe #7 (containing #56), again, indicates the possibility of having an additional short step in the *M-H* curve for small J_2 [see Fig. 5(d)]. Another phase #20, which corresponds to $M = 1/2$, begins to develop in a small triangle region that borders #2, #3, and #4. On the other hand, with a slightly larger $J_4 = -0.125$, both #7 and #12 expand and a new phase #10 appears along #3–#4 border. In this case, one can see four transitions (five phases) in the *M-H* curve as shown in Fig. 5(d). It is worth noting that, coincidentally, while all three curves contain the same magnetization steps, for $M = 0$ and 0.5, the orderings for $J_2 > 0.1$ are in fact in different phases (#12 and #20, respectively).

In the bottom row [i.e., Figs. 5(e)–5(h)], a larger J_3 further stabilizes #1, #3, and #4, and this case, at the expense of #2, as shown in Fig. 5(e), and it would require a larger J_4 to introduce new phases, as shown in Figs. 5(g) and 5(h). For $J_4 = -0.35$, phases #12, #20, and #56 favored by J_4 expand into the positive J_2 region. For $J_2 < 0.1$, the pattern of involved phases closely resembling that of Fig. 5(c) reappears.

IV. A CASE STUDY: $ErGa_2$

To gain more insight, we look into a realistic system $ErGa_2$ using first-principles calculations. We find that the interplanar interactions are dominated by the ferromagnetic NN coupling along c, which allows us to reduce the 3D Hamiltonian to an effective 2D Ising model. The calculated parameters of this model (which implicitly combine intraplanar and interplanar interactions) are shown in Table I.

Figure 6(a) presents a comparison between the experimental *M-H* curves measured at 1.5 K [18] and those derived using our parameters, J_i^{DFT}, extracted from the DFT calculations in
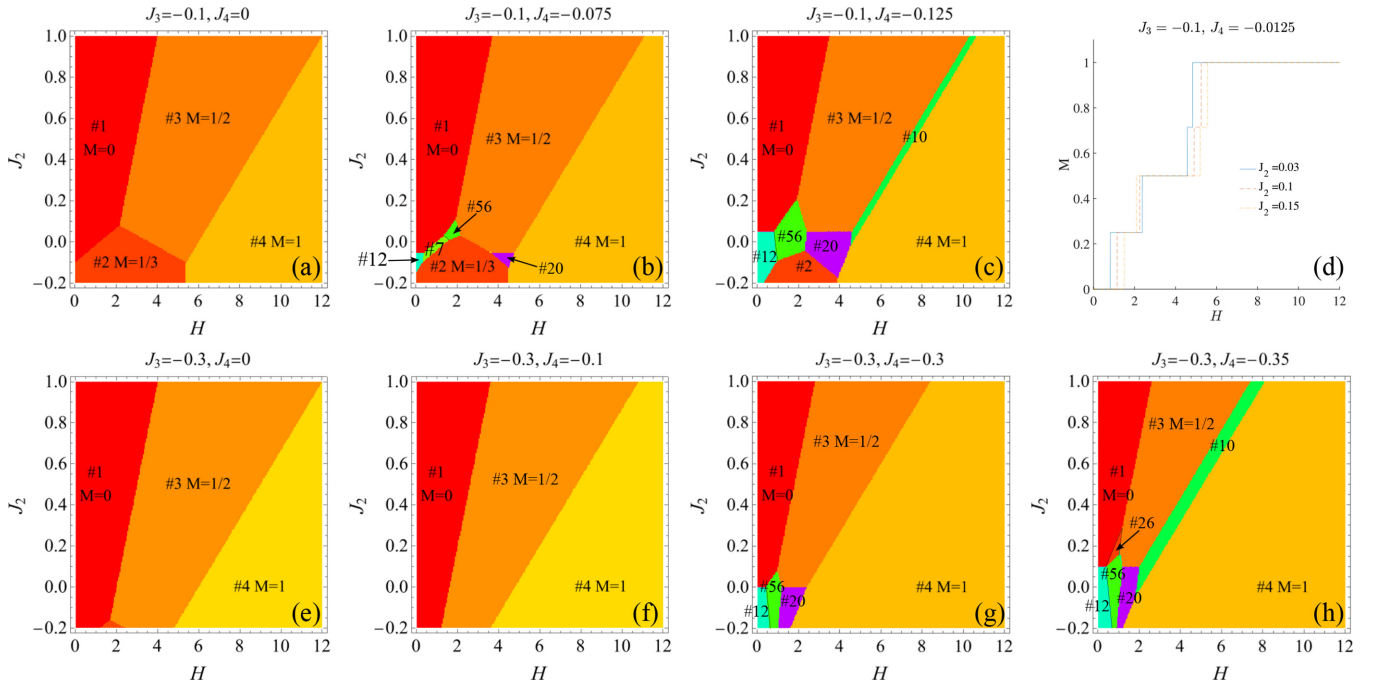
FIG. 5. Phase diagrams and magnetization vs applied field.

Table I. The agreement is very good, apart from an overall overestimation of ~30%, as is common in DFT calculation. Particularly, the qualitative behaviors are accurately captured, as both feature two distinct, well-defined steps of $M = 0.5$ and 1 that correspond to phases #3 and #4, respectively, and the ratio between the two transition fields $H_2/H_1 \sim 3$, as discussed in Ref. [18], is also well reproduced.

It is worth noting that, owing to the strong easy-axis anisotropy on the Er sites, one would anticipate the transitions at H_1, and H_2 to be abrupt. The observed finite widths may be due to sample quality, for instance, inhomogeneity. However, another interesting possibility is that crossover regions between ≈ 0.6 and ≈ 1 T, and between ≈ 2 and ≈ 1 T, hide inside unresolved narrow steps.

Indeed by observing the pattern in Fig. 5(b) and exploring parameters near our DFT results, we managed to unveil two additional steps—one corresponds to #7 and the other to #2 located within a very narrow range of field around H_1—simply by slightly reducing the NN J_3 (J_4) from -0.17 (0.075) to -0.09 (0.055) as listed in Table I and labeled J_i^{set1}.

TABLE I. First to fourth NN interactions and their distances d. J_i^{DFT} ($i = 1$–4) are obtained by fitting into DFT calculations. J_i^{set1} and J_i^{set2} are tuned manually around the DFT parameters to explore the possible hidden steps. All values are divided by $J_1^{DFT} = 0.285$ meV.

iNN	distance (Å)	$J_i^{DFT}/|J_1^{DFT}|$	$J_i^{set1}/|J_1^{DFT}|$	$J_i^{set2}/|J_1^{DFT}|$
1	4.186	1	1	1
2	7.250	0.055	0.055	0.140
3	8.372	-0.173	-0.09	-0.019
4	11.075	-0.075	-0.057	-0.025

With a slightly larger deviation from the J_i^{DFT} parameter set, we were also able to find another set of parameters J_i^{set2} that produces an additional short intermediate state between the #3 to #4 transition. Although the transition fields no longer coincide as closely, the qualitative trend remains the same (i.e., $H_2 \sim 3H_1$). Based on this analysis, we believe that in a more accurate experiment with better samples, it might be possible to resolve two or more additional steps. It is also important to note that the RKKY interaction, in reality, is long-range oscillating and can potentially produce even more states.

Second, the experimental data also reveal narrow yet distinct hysteresis loops during both transitions. To understand the possible origin of hysteresis, we discuss the issue from
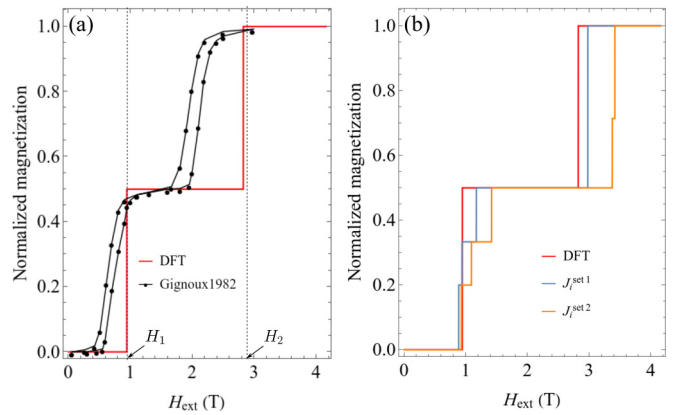
FIG. 6. The comparison of field-dependent magnetization between (a) DFT and experimental data taken from Ref. [18], and (b) DFT and two additional sets of manually tuned parameters. The exact field strengths are estimated based on experimental moment $M = 9.5 \mu_B$.

two different aspects. If the intermediate states #7 and #2 exist as we predicted, then direct (2nd order) transition from #1 to #7 or #2 to #3 is prohibited, as the symmetries of these states are incompatible. This manifests itself in that these transitions require simultaneous multiple spin-flips, and nucleation of finite-size domains of a new phase; i.e., they are the 1st kind and potentially hysteretic.

On the contrary, the transition between #1 and #3, as well as between #3 and #4, can be achieved by sequentially flipping the spin one by one. In this case, one can easily establish the order of the transitions by the critical field necessary to flip one spin, with the field needed to flip all affected spins.

For instance, for the #1 to #3 transition, one can simply estimate the energy cost of flipping one spin in the entire lattice under the field H_1', which has the analytic energy expression

$$E_{1+1\text{flip}} - E_1 = 4J_1 + 4J_2 - 12J_3 + 8J_4 - 2H_1' \quad (5)$$

and for the full transition at H_1 we have

$$E_3 - E_1 = 4J_1 + 4J_2 + 8J_4 - 2H_1. \quad (6)$$

Similarly, for the #3 to #4 transition, we have the following for the energy cost of flipping one spin in #3 under H_2',

$$H_{3+1\text{flip}} - H_3 = 12J_1 + 12J_2 - 12J_3 + 24J_4 - 2H_2', \quad (7)$$

and the energy for the full transition,

$$H_4 - H_3 = 12J_1 + 12J_2 + 24J_4 - 2H_2. \quad (8)$$

Interestingly, the difference between Eqs. (5) and (6), as well as between Eqs. (7) and (8), depends only on J_3. Using our DFT parameter J_3^{DFT}, we find that flipping one single spin in both cases requires a larger field than triggering the full transitions (i.e., $H_1' > H_1$ and $H_2' > H_2$), and as a result, both transitions are predicted to be hysteretic.

V. CONCLUSIONS

In conclusion, we have studied the effect of further neighbors on metamagnetic transitions in the classical Ising model on the triangular lattice. We determine the phase diagrams for two scenarios through a comprehensive examination of magnetic energy comparisons of all possible magnetic states allowed within a supercell no longer than 8th NN, as well as including one additional longer-ranged order discussed in the earlier literature. We have considered two qualitatively different sets of exchange Hamiltonians: one where all exchange interactions are antiferromagnetic which hosts the richest phase diagram with high frustrations and multiple near-degenerate phases. We discussed how these degeneracies are lifted by further-neighbor interactions, and lead to exceptionally rich phase diagrams with up to 56 phases. The second case, motivated by our DFT calculations for ErGa$_2$, is introduced to mimic the Ruderman-Kittel-Kasuya-Yosida (RKKY) type of interaction where the sign of interactions varies with distance. Furthermore, we present a case study on a real-world system ErGa$_2$. By incorporating our first-principles-based exchange parameters into the I-3 model, we were able to reproduce the experimentally observed magnetization steps. With the help of the analysis for the second scenario, we also predict the possibility of additional steps that could be revealed in better samples.

[1] L. Balents, Nature (London) **464**, 199 (2010).

[2] L. Santos, M. A. Baranov, J. I. Cirac, H.-U. Everts, H. Fehrmann, and M. Lewenstein, Phys. Rev. Lett. **93**, 030601 (2004).

[3] T.-H. Han, J. S. Helton, S. Chu, D. G. Nocera, J. A. Rodriguez-Rivera, C. Broholm, and Y. S. Lee, Nature (London) **492**, 406 (2012).

[4] S. Nakatsuji, Y. Nambu, H. Tonomura, O. Sakai, S. Jonas, C. Broholm, H. Tsunetsugu, Y. Qiu, and Y. Maeno, Science **309**, 1697 (2005).

[5] M. R. Norman, Rev. Mod. Phys. **88**, 041002 (2016).

[6] K. Zhao, H. Deng, H. Chen, K. A. Ross, V. Petříček, G. Günther, M. Russina, V. Hutanu, and P. Gegenwart, Science **367**, 1218 (2020).

[7] L. Landau and E. Lifshitz, *Statistical Physics: Volume 5* (Elsevier Science, Amsterdam, 2013), p. 498.

[8] M. A. Ruderman and C. Kittel, Phys. Rev. **96**, 99 (1954).

[9] T. Kasuya, Prog. Theor. Phys. **16**, 45 (1956).

[10] J. H. Van Vleck, Rev. Mod. Phys. **34**, 681 (1962).

[11] G. H. Wannier, Phys. Rev. **79**, 357 (1950).

[12] Y. Tanaka and N. Uryû, J. Phys. Soc. Jpn. **39**, 825 (1975).

[13] B. Metcalf, Phys. Lett. A **46**, 325 (1974).

[14] J. Chen, W. Z. Zhuo, M. H. Qin, S. Dong, M. Zeng, X. B. Lu, X. S. Gao, and J. M. Liu, J. Phys.: Condens. Matter **28**, 346004 (2016).

[15] N. Uryû and Y. Tanaka, Phys. Lett. A **51**, 451 (1975).

[16] T. H. Tsai, J. A. Gerber, J. W. Weymouth, and D. J. Sellmyer, J. Appl. Phys. **49**, 1507 (1978).

[17] T. H. Tsai and D. J. Sellmyer, Phys. Rev. B **20**, 4577 (1979).

[18] M. Doukourè and D. Gignoux, J. Magn. Magn. Mater. **30**, 111 (1982).

[19] R. D. D. Reis, L. M. D. Silva, A. O. D. Santos, A. M. Medina, L. P. Cardoso, and F. C. Gandra, J. Alloys Compd. **582**, 461 (2014).

[20] R. D. dos Reis, L. M. da Silva, A. O. dos Santos, A. M. N. Medina, L. P. Cardoso, and F. G. Gandra, J. Phys.: Condens. Matter **22**, 486002 (2010).

[21] See Supplemental Material at http://link.aps.org/supplemental/10.1103/PhysRevB.110.014418 for a comprehensive compilation of magnetic patterns identified as ground states or closely approaching ground state energies.

[22] M. Diviš, M. Richter, J. Forstreuter, K. Koepernik, and H. Eschrig, J. Magn. Magn. Mater. **176**, L81 (1997).

[23] A. R. Ball, D. Gignoux, D. Schmitt, and F. Y. Zhang, J. Magn. Magn. Mater. **140**, 1121 (1995).

[24] T. Horiguchi and T. Morita, Phys. Lett. A **41**, 9 (1972).

[25] G. Kresse and J. Furthmüller, Phys. Rev. B **54**, 11169 (1996).

[26] P. E. Blöchl, Phys. Rev. B **50**, 17953 (1994).

[27] G. Kresse and D. Joubert, Phys. Rev. B **59**, 1758 (1999).

[28] J. P. Perdew, K. Burke, and M. Ernzerhof, Phys. Rev. Lett. **77**, 3865 (1996).

[29] V. I. Anisimov and O. Gunnarsson, Phys. Rev. B **43**, 7570 (1991).